UC San Diego

Title

Proregenerative extracellular matrix hydrogel mitigates pathological alterations of pelvic skeletal muscles after birth injury

Permalink

https://escholarship.org/uc/item/8x6230kh

Journal

Science Translational Medicine, 15(707)

ISSN

1946-6234

Authors

Duran, Pamela
Boscolo Sesillo, Francesca
Cook, Mark
et al.

Publication Date

2023-08-02

DOI

10.1126/scitranslmed.abj3138

Peer reviewed

Proregenerative extracellular matrix hydrogel mitigates pathological alterations of pelvic skeletal muscles after birth injury

Pamela Duran[1,2], **Francesca Boscolo Sesillo**[2,3], **Mark Cook**[4], **Lindsey Burnett**[3], **Shawn A. Menefee**[5], **Emmy Do**[6], **Saya French**[6], **Gisselle Zazueta-Damian**[5], **Monika Dzieciatkowska**[7], **Anthony J. Saviola**[7], **Manali M. Shah**[1], **Clyde Sanvictores**[8], **Kent G. Osborn**[9], **Kirk C. Hansen**[7], **Matthew Shtrahman**[2,10], **Karen L. Christman**[1,2,*], **Marianna Alperin**[2,3,*]

[1]Shu Chien-Gene Lay Department of Bioengineering, University of California San Diego, La Jolla, CA 92093, USA.

[2]Sanford Consortium for Regenerative Medicine, University of California San Diego, La Jolla, CA 92037, USA.

[3]Department of Obstetrics, Gynecology, and Reproductive Sciences, Division of Female Pelvic Medicine and Reconstructive Surgery, University of California San Diego, La Jolla, CA 92093, USA.

[4]Department of Integrative, Biology and Physiology, University of Minnesota, Minneapolis, MN 55455, USA.

[5]Department of Obstetrics and Gynecology, Division of Female Pelvic Medicine and Reconstructive Surgery, Kaiser Permanente, San Diego, CA 92110, USA.

*Corresponding author. christman@eng.ucsd.edu (K.L.C.); malperin@health.ucsd.edu (M.A.).

Supplementary Materials

This PDF file includes:

Materials and Methods

Fig. S1 to S21

Table S1 to S11

References (57–63)

Other Supplementary Material for this manuscript includes the following:

Data file S1

MDAR Reproducibility Checklist

[6]Department of Biology, University of California San Diego, La Jolla, CA 92093, USA.

[7]Department of Biochemistry and Molecular Genetics, School of Medicine, University of Colorado, Aurora, CO 80045, USA.

[8]Department of Physics, University of California San Diego, La Jolla, CA 92093, USA.

[9]Center for Veterinary Sciences and Comparative Medicine, Division of Comparative Pathology and Medicine, University of California San Diego, La Jolla, CA 92093, USA.

[10]Department of Neurosciences, University of California San Diego, La Jolla, CA 92093, USA.

Abstract

Pelvic floor disorders, including pelvic organ prolapse and urinary and fecal incontinence, affect millions of women globally and represent a major public health concern. Pelvic floor muscle (PFM) dysfunction has been identified as one of the leading risk factors for the development of these morbid conditions. Childbirth, specifically vaginal delivery, has been recognized as the most important potentially modifiable risk factor for PFM injury; however, the precise mechanisms of PFM dysfunction after parturition remain elusive. In this study, we demonstrated that PFMs exhibit atrophy and fibrosis in parous women with symptomatic pelvic organ prolapse. These pathological alterations were recapitulated in a preclinical rat model of simulated birth injury (SBI). The transcriptional signature of PFMs after injury demonstrated an impairment in muscle anabolism, persistent expression of genes that promote extracellular matrix (ECM) deposition, and a sustained inflammatory response. We also evaluated the administration of acellular injectable skeletal muscle ECM hydrogel for the prevention of these pathological alterations. Treatment of PFMs with the ECM hydrogel either at the time of birth injury or 4 weeks after injury mitigated PFM atrophy and fibrosis. By evaluating gene expression, we demonstrated that these changes are mainly driven by the hydrogel-induced enhancement of endogenous myogenesis, ECM remodeling, and modulation of the immune response. This work furthers our understanding of PFM birth injury and demonstrates proof of concept for future investigations of proregenerative biomaterial approaches for the treatment of injured pelvic soft tissues.

INTRODUCTION

elvic organ prolapse (POP) and urinary and fecal incontinence disproportionately affect cis-women. The prevalence of these conditions, collectively known as pelvic floor disorders (PFDs), ranges from about 25% of the female population in the United States and China to about 50% in Australia and Japan (1–4). Although not lifethreatening, PFDs represent a major public health concern because of their negative impact on quality of life, associated morbidities, and economic burden. The pelvic floor supports the abdominal and pelvic organs by opposing gravitational forces and intra-abdominal pressure, aids in urinary and fecal continence, and contributes to sexual function and parturition. The complex pelvic supportive system includes the bony pelvis, vagina, connective tissues, superficial perineal muscles, and pelvic floor muscles (PFMs) that are composed of the levator ani and the coccygeus muscles. PFM dysfunction has been consistently identified as one of the leading risk factors for the development of symptomatic PFDs (5, 6), highlighting the need to investigate mechanisms that govern PFM deterioration.

Epidemiological studies have unequivocally identified vaginal childbirth as the leading risk factor associated with PFM injury (6). Despite this, the precise mechanisms of PFM dysfunction in parous women remain elusive (6). In addition, alterations in the intrinsic PFM components have not been well characterized in women with PFDs. Thus, we sought to compare the morphological properties of PFMs procured from vaginally parous women with symptomatic POP and from age-matched nulliparous and parous cadaveric donors without history of PFDs.

During vaginal delivery, PFMs are subjected to mechanical strains that exceed the upper physiological limit (about 60%), beyond which appendicular skeletal muscle injury ensues (7). On the basis of computational models of human fetal delivery, the enthesial region of the pubovisceralis portion of the levator ani complex experiences the highest strains, up to 300% (8). These excessive strains have been presumed to cause radiologically detected avulsions; however, this phenotype is not present in all women with PFM dysfunction (9, 10). Because of ethical and technical constraints associated with directly probing PFMs in living women, animal models are essential to study mechanisms of PFM birth injury. We previously validated a rat model for the study of the human PFMs (11) and observed similar stretch ratios of the rat and human pubocaudalis/pubovisceralis during vaginal distention (12). In the rat PFMs, such strains led to sarcomere hyperelongation and myofibrillar disruption (12), major causes of mechanical skeletal muscle injury (13). Studies of the limb muscles identified that inflammation after acute injury negatively affects muscle recovery (13, 14). In contrast, the downstream events after PFM birth injury have not yet been determined. In the current study, we examined early and delayed PFM responses to simulated birth injury (SBI) using the rat model.

Beyond the lack of fundamental knowledge regarding tissue and cellular alterations that govern PFM dysfunction, there are currently few strategies to preempt the maladaptive recovery of PFMs after birth injury. PFM rehabilitation, recommended to offset PFM weakness in pregnant and postpartum women, is associated with poor adherence (15). Furthermore, the existing treatments for PFM dysfunction and the associated PFDs are plagued with high failure rates (16, 17), and the only preventative strategy for maternal birth injury, cesarean section, is associated with substantial distinct morbidities (18). Given the rising prevalence of PFDs, preventative and therapeutic approaches are urgently needed to address this public health problem. One tactic may be to potentiate constructive remodeling of PFMs after birth injury to prevent PFM deterioration. We and others have previously demonstrated that a decellularized porcine skeletal muscle extracellular matrix (ECM) hydrogel (SKM) increases recruitment of muscle progenitors and expression of myogenic markers compared with a collagen hydrogel (19–21). SKM is superior to nonmuscle ECM hydrogel in promoting constructive remodeling in ischemic skeletal muscles through up-regulation of myogenesis and blood vessel development (22). Therefore, our last objective was to investigate the efficacy of SKM, administered at two clinically relevant time points, for the prevention and treatment of the pathological PFM alterations consequent to birth injury.

In this study, we observed substantial PFM atrophy and fibrosis in samples from parous women with POP compared with PFMs procured from age-comparable nulliparous

and parous cadaveric donors without history of PFDs. These pathological alterations, replicated in the SBI preclinical model, appeared to be governed by the impairment in muscle anabolism, persistent expression of genes that promote ECM deposition, and sustained inflammatory response. The acellular proregenerative biomaterial prevented and mitigated the pathological PFM alterations in the preclinical model through enhancement of myogenesis, ECM remodeling, and modulation of the immune response. Our findings provide a rationale for the further investigation of tissue-specific proregenerative biomaterials as a preventative therapy after birth injury.

RESULTS

PFMs in women with symptomatic POP demonstrate substantial muscle atrophy and fibrosis

We biopsied the pubovisceralis portion of levator ani from vaginally nulliparous (VN) and parous (VP) cadaveric donors without history of PFDs and from parous women undergoing surgery for symptomatic POP (fig. S1). All cadaveric donors were White/non-Hispanic, whereas in the POP group, participants included White/non-Hispanic (73.9%), White/Hispanic (17.4%), and Asian (8.7%). The groups did not differ with respect to age (VN, 72.0 ± 7.5 years; VP, 73.0 ± 13.3 years; POP, 69.9 ± 3.1 years; $P = 0.6$) or body mass index (VN, 25.4 ± 2.4 kg/m^2; VP, 21.3 ± 4.5 kg/m^2; POP, 27.1 ± 1.1 kg/m^2; $P = 0.5$). The median parity was 3 (1 to 7). We assessed fiber shape and packing, collagen content (fibrosis), fiber area (atrophy), centralization of nuclei (degeneration-regeneration), and intramuscular fat content (fatty degeneration).

In the POP group, 20% of biopsies contained no myofibers on histological examination. In the remaining biopsies, myofibers exhibited disrupted fiber packing, whereas in the control groups (VN and VP), moderate fiber packing density was observed (Fig. 1A). Histological parameters (Fig. 1, B to E) were similar between VN and VP groups without history of PFDs. A significant decrease in fiber cross-sectional area was found in the POP group relative to the controls ($P < 0.0001$ versus VN and VP; Fig. 1B). The smaller fiber size was accompanied by increased collagen content in the POP group compared with the controls ($P = 0.001$ versus VN and VP; Fig. 1C). The proportion of centralized nuclei ($P = 0.4$ versus VN and $P = 0.13$ versus VP; Fig. 1D) or intramuscular fat content ($P = 0.9$ versus VN and VP; Fig. 1E) did not differ between groups. Together, our results demonstrated atrophy and fibrotic degeneration of PFMs in parous women with symptomatic POP.

We then investigated whether any of the examined demographic factors in the POP group could contribute to the severity of atrophy and fibrosis. No correlations were observed between the number of births, age, or body mass index and the extent of pathological alterations identified (table S1).

The rat model of SBI replicates pathological alterations observed in parous women with POP

We have previously identified that the pubocaudalis component of rat levator ani, analogous to the human pubovisceralis, undergoes the largest macro- and microscopic structural

alteration acutely in response to SBI (12). To replicate the circumferential and downward strains associated with parturition, a transurethral weighted modified catheter was inserted into the vagina. The balloon was inflated to 5 ml and left in place for 2 hours [the median duration of the second stage of labor (23)], after which it was pulled through the introitus. To assess the impact of SBI, we assessed fibersize, collagen content, and arteriole density, given that revascularization is important for muscle regeneration (14), at subacute (4 weeks after SBI) and long-term (8 weeks after SBI) time points. We first compared 3- and 5-month-old uninjured controls to rule out possible age-related differences at the time of SBI (3 months old) and 8 weeks after SBI (5 month old). No significant differences were observed between these groups in the PFM fiber area ($P = 0.1$), collagen content ($P = 0.3$), or arteriole density ($P = 0.4$) (fig. S2, A to C). Thus, 3-month-old uninjured controls were used to assess changes in the morphological muscle parameters consequent to birth injury.

We observed a significant decrease in PFM fiber area 4 weeks after injury compared with uninjured controls ($P < 0.0001$), with fiber area distribution enriched with smaller fibers (Fig. 2, A and B) in injured pubocaudalis. To determine whether changes in fiber size at this subacute time point were due to muscle atrophy or ongoing muscle regeneration, we assessed the centralization of nuclei, a marker of regeneration (14). The number of fibers with centralized nuclei was increased 4 weeks after SBI compared with controls ($P = 0.02$), indicating ongoing regeneration (Fig. 2C). By 8 weeks after birth injury, percent centralized nuclei returned to baseline ($P = 0.7$). Despite an increase in cross-sectional area at this longer-term time point compared with 4 weeks after SBI ($P < 0.0001$; Fig. 2, A and B), fiber size remained smaller than in uninjured controls ($P < 0.0001$). The return of centralized nuclei to baseline values with persistent smaller fiber size at 8 weeks after SBI suggested that birth injury led to PFM atrophy. Because myofiber atrophy is often accompanied by the pathological thickening of endo- and peri-mysium, we investigated whether the total amount of collagen, the major constituent of the intramuscular ECM, was altered by birth injury. We observed an increase in the pubocaudalis collagen content 4 and 8 weeks after SBI compared with uninjured controls ($P = 0.02$ and $P = 0.03$, respectively; Fig. 2, D and E). These results suggested that in addition to muscle atrophy, birth injury also led to PFM fibrosis. Although fiber cross-sectional area increased at 12 weeks [1810 (71.54 to 4937) μm^2] compared with 8 weeks after SBI ($P < 0.0001$), fiber size remained smaller relative to uninjured controls ($P < 0.0001$). The intramuscular collagen content remained elevated at 12 weeks ($3.9 \pm 0.04\%$) relative to uninjured controls ($P < 0.0001$).

With respect to the intramuscular vasculature, the total arteriole density increased at 4 ($P = 0.01$) and 8 weeks ($P = 0.02$) after SBI relative to uninjured controls (Fig. 2, F and G), with return to baseline by 12 weeks (7.4 ± 1.26 arterioles/mm^2, $P = 0.18$ versus controls). We then compared the distribution of arterioles of various diameters between groups (24). The smaller arterioles (11 to 25 μm) were increased at 4 ($P = 0.0005$), 8 ($P < 0.0001$), and 12 weeks after SBI (6.02 ± 0.74 arterioles/mm^2, $P = 0.01$) compared with uninjured controls (Fig. 2H), with similar density of larger arterioles in all groups ($P > 0.99$). The above findings indicated that birth injury altered PFM vascularization, consistent with the observations in injured fibrotic appendicular muscles (25).

Myogenesis occurs within 1 week after SBI in rats

To identify potential mechanisms involved in the long-term pathological alterations of PFMs, we elucidated cellular events after SBI. The unperturbed pubocaudalis demonstrated tightly packed myofibers (Fig. 3A). One day after SBI, widespread myofiber death was observed, followed by accumulation of cellular infiltrate [mono-nuclear phagocytes (macrophages) and neutrophils] 3 days after injury (Fig. 3A and fig. S3). Regenerating myofibers, identified by centralized nuclei, were observed 7 days after injury. Endomysial thickening and continuous cellular infiltration were noted at 10 days after SBI (Fig. 3A).

Because muscle stem cells (MuSCs) are indispensable for muscle regeneration, we next investigated their differentiation and self-renewal capacities at 1, 3, 7, and 10 days after SBI. In injured appendicular muscles, MuSCs replace or repair the damaged muscle by differentiating into myoblasts and forming new myofibers (3 to 4 days after injury) or fusing with preexisting ones, whereas a portion of MuSCs self-renews to replenish the stem cell pool (5 to 7 days after injury) (26, 27). The peak density of differentiated myogenin+ MuSCs was observed 3 days after SBI ($P = 0.01$ versus uninjured control), with return to baseline at 7 days (Fig. 3B). The number of quiescent and self-renewing Pax7+ MuSCs increased substantially 7 days after SBI relative to uninjured controls ($P < 0.001$), returning to baseline 10 days after birth injury (Fig. 3C). The rapid differentiation of MuSCs after birth injury was further confirmed by the presence of the embryonic myosin heavy chain+ de novo or fused myofibers as early as 3 days after SBI (fig. S4). Together, these data indicated that after birth injury, PFM myogenesis followed the same time course as that observed in injured appendicular skeletal muscles (27). Thus, disturbance in the early regenerative process is an unlikely mechanism behind the long-term atrophic and fibrotic PFM phenotype consequent to birth injury.

Sustained inflammatory response of the PFMs follows SBI in rats

To further decipher the mechanisms underlying the observed muscle phenotype, we examined changes in gene expression associated with PFM injury. A custom 150-gene Nanostring panel included pathways known to regulate appendicular muscles' response to injury: immune response, myogenesis, muscle anabolism and catabolism, ECM remodeling, neovascularization, and neuromuscular junction development and maturation (table S2). We assessed the transcriptional signature of the pubocaudalis at 1, 3, 7, 10, 31, and 35 days after SBI. To determine patterns across the postinjury continuum, principal components analyses were performed for all assayed transcripts together (Fig. 4A) and for each individual pathway (fig. S5, A to G). As expected, principal component 1 that accounts for the highest variability was attributable to the pubocaudalis response to birth injury, with progressive return toward the uninjured state during the recovery period (Fig. 4A and fig. S5, A to F).

We then evaluated differentially expressed genes in each pathway to determine longitudinal alterations from the uninjured state (Fig. 4, B to G, and tables S3 to S8). Figure S6 demonstrates the gene expression profile at each time point. For the immune response pathway (Fig. 4B), proinflammatory genes increased after injury, with sustained up-regulation of *interleukin-1 beta* (*Il1b*), *interferon regulatory factor 5* (*Irf5*), and *t-box transcription factor 21* (*Tbx21*) until day 31 after SBI. In contrast, genes associated with

the proregenerative phase were up-regulated only until day 7. *Forkhead box P3* (*Foxp3*), which encodes the forkhead box protein P3, a transcription factor for regulatory T cells involved in the shift toward the proregenerative response, was down-regulated at all time points examined after SBI. For the myogenic pathway (Fig. 4C), expression of genes related to muscle structure decreased acutely, returning to the uninjured values by 31 days. In contrast, genes coding for muscle transcription factors had variable expression. *Myogenin* (*Myog*), *myosin heavy chain 3* (*Myh3*), and *paired box 7* (*Pax7*) expression decreased 1 day after injury, followed by increased expression of *Myog* and *Myh3* at 3 days and *Pax7* at 7 days after SBI, consistent with the differentiation/self-renewal pattern observed by immunostaining (Fig. 3, B and C). For muscle anabolism pathways (Fig. 4D), we observed down-regulation of all genes related to the protein kinase B (AkT)/mammalian target of rapamycin (mTOR) signaling until day 10, with decreased expression of its downstream targets, *ribosomal protein s6 kinase beta-1* (*Rps6kb1*) and *eukaryotic translation initiation factor 4e* (*Eif4e*), until day 31. For muscle catabolism pathways, the majority of genes were decreased at all time points, with the exception of *cathepsin l* (*Ctsl*), involved in protein and lysosomal degradation, that increased at days 1 and 3 (Fig. 4D). For the ECM pathways (Fig. 4E), increased expression of ECM remodeling genes *platelet-derived growth factor receptor alpha* (*Pdgfra*), *collagen type 1 alpha 1 chain* (*Col1a1*), and *collagen type 3 alpha 1 chain* (*Col3a1*) was observed at 7 and 3 to 10 days, respectively, whereas *transforming growth factor beta 1* (*Tgfb1*) and *tissue inhibitor of metalloproteinases 1* (*Timp1*) continued to be up-regulated until 31 days after injury. For vascularization pathways, genes that directly promote vascularization were decreased at the acute (1 to 10 days) and subacute (31 days) time points, whereas genes that inhibit vascularization were increased at 1 to 10 days (Fig. 4F). Genes related to neuromuscular junction development [*neuregulin* (*Nrg1*) and *tenascin C* (*Tnc*)] and maturation [*amyloid beta precursor protein* (*App*)] were increased starting on days 1 and 7, respectively (Fig. 4G). Overall, on the basis of this gene expression analysis, birth injury led to impairment in PFM anabolism, sustained up-regulation of genes that promote ECM deposition, and persistent inflammatory response.

To corroborate the persistent up-regulation of inflammatory genes after birth injury, we investigated changes in immune cellular populations using flow cytometry. The population of $CD45^+$ cells increased at the earlier time points after SBI relative to uninjured controls ($P < 0.01$), with return to baseline by 31 days (Fig. 5, A and B). The number of $CD45^+CD68^+$ cells (macrophages) increased significantly within 7 days after injury ($P < 0.0001$; Fig. 5, A and C). Further analyses revealed that inflammatory ($CD45^+CD68^+iNOS^+$) macrophages (28) increased at 3 days after SBI and continued to be higher than in uninjured controls at 7 days ($P < 0.0001$; Fig. 5, A and D), whereas anti-inflammatory ($CD45^+CD68^+iNOS^-$) macrophages did not rise above the control values until day 7 after birth injury ($P < 0.0001$; Fig. 5, A and E). T helper cells ($CD45^+CD4^+$; Fig. 5, F and G) were increased at 3 days after SBI relative to uninjured controls ($P = 0.006$). Within these $CD45^+CD4^+$ cells, a persistent increase in the proinflammatory ($CD45^+CD4^+GATA3^-$) subpopulation (29) was observed throughout the 31-day recovery period ($P = 0.016$; Fig. 5, F and H), whereas the anti-inflammatory ($CD45^+CD4^+GATA3^+$) subpopulation exceeded that in the uninjured controls only at 3 days after injury ($P = 0.006$; Fig. 5, F and I).

We performed a correlation analysis between the immune response genes known to be expressed by macrophages [*nitric oxide synthase 1* (*Nos*) and *arginase 1* (*Arg1*)] and T helper cells [*Tbx21* and *GATA binding protein 3* (*Gata3*)] and the immune cellular populations identified in PFMs. We observed a positive correlation between subpopulations of macrophages and T helper cells with their respective canonical genes (table S9). In particular, *Tbx21* (T helper 1 inflammatory cells) was persistently up-regulated after birth injury, correlating with the long-term increase in CD45$^+$CD4$^+$ GATA3$^-$ cells after SBI.

SKM prevents PFM atrophy and mitigates fibrosis when administered at the time of SBI

Given incomplete PFM recovery from SBI in the rat model, we went on to investigate whether SKM, an ECM hydrogel derived from decellularized porcine skeletal muscle, could potentiate muscle recovery when injected directly into pubocaudalis at the time of SBI. We hypothesized that SKM's immunomodulatory properties would counteract the sustained inflammatory response in PFMs by inducing an early transition to the proregenerative environment (22). Injection of saline served as an experimental control (Fig. 6A). Because fiber area and collagen content were quantified 4 weeks after SBI + injection, data from animals at this time point without any injection were also used for comparison, given the reproducibility of our model (fig. S7).

Although saline increased fiber area compared with untreated SBI ($P < 0.0001$), SKM resulted in a greater increase in fiber area compared with saline ($P < 0.0001$), with return of fiber size to the uninjured values (SBI + SKM versus uninjured controls: $P > 0.99$; Fig. 6B). SKM also lowered collagen deposition relative to untreated SBI ($P = 0.02$), bringing intramuscular collagen content down to the value of uninjured pubocaudalis ($P = 0.6$). Similar collagen deposition response was observed in the SBI + saline group ($P = 0.5$; Fig. 6C). These results suggested that SKM could prevent PFM atrophy and mitigate fibrotic degeneration consequent to birth injury. With respect to vascularization, the arteriole density in the SKM group did not differ significantly from saline ($P = 0.5$), untreated SBI ($P = 0.4$), or uninjured controls ($P = 0.1$). Unexpectedly, the arteriole density was higher in the saline group compared with uninjured controls ($P = 0.01$; Fig. 6D). The smaller arterioles (11 to 25 μm) decreased in SKM group relative to untreated SBI ($P = 0.002$). This decrease was not statistically different compared to saline ($P = 0.09$; Fig. 6E). In addition, the smaller arterioles were not different in the saline group in relation to untreated SBI ($P = 0.2$; Fig. 6E). The above suggests that SKM mitigates the arteriole alterations of PFMs observed after birth injury.

We went on to assess transcriptional regulation of the changes in the PFM phenotype induced by SKM injection. Pubocaudalis was harvested at 3 or 7 days after SBI + injection (Fig. 6A). These time points correspond to the early inflammatory response and peak cell infiltration into the material, respectively. The Nanostring panel described above (table S2) was used for comparisons with uninjured controls and the untreated SBI group. On the basis of the principal components analysis, SKM, saline, and untreated SBI groups did not cluster separately at either time point (Fig. 6, F and G); however, several genes were differentially expressed (figs. S8 and S9). Clustered heatmaps of the differentially expressed

genes between SKM and saline representing the fold change relative to untreated SBI are shown in Fig. 6 (H and I), with pairwise comparisons summarized in fig. S10.

At 3 days after SBI, SKM down-regulated *Nos2*, *Il1b*, chemokine (*c-x-c motif*) *ligand 1* (*Cxcl1*), *chemokine (c-c motif) ligand 2* (*Ccl2*), and *chemokine (c-c motif) ligand 3* (*Ccl3*) genes associated with a proinflammatory environment. We also observed up-regulation of genes associated with MuSC pool expansion (*Pax7* and *Myf5*) and a trend toward up-regulation of a muscle transcription factor that encodes for de novo or fused myofibers (*Myh3*, $P = 0.06$ versus saline). The expression of the genes associated with ECM remodeling was decreased at 3 (*Mmp8* and *Mmp9*) and 7 (*Ccn2* and *Itga1*) days after injury. *Col1a1* expression trended down at 7 days after SBI ($P = 0.07$ versus saline). Expression of *vascular endothelial growth factor A* (*Vegfa*) and *vascular endothelial growth factor receptor 2* (*Kdr*), associated with vascularization, was decreased at both time points. *Tnc*, involved in the development of neuromuscular junctions, was down-regulated at 7 days. Together, our results indicated that compared with saline, SKM treatment at the time of birth injury up-regulated genes in the myogenesis pathway early on and decreased the expression of genes related to inflammation and ECM remodeling.

Delayed injection of SKM prevents PFM atrophy and mitigates fibrosis in rats

Given translational relevance of PFM treatment around the time of a routine postpartum visit, we next evaluated whether SKM injection 4 weeks after SBI (Fig. 7A) could prevent PFM atrophy and fibrosis consequent to birth injury. SKM potentiated PFM long-term recovery, as evident from the increased fiber area compared with saline at 8 weeks after SBI ($P < 0.0001$; Fig. 7B). SKM administration resulted in a fiber area greater than that of the uninjured controls ($P < 0.0001$; Fig. 7B). Saline also increased fiber area compared with untreated SBI ($P < 0.0001$) but failed to return fiber size to the uninjured values ($P < 0.0001$). To assess whether the proremodeling changes induced by the biomaterial were sustainable, we analyzed fiber area at 8 weeks after injection, corresponding to 12 weeks after SBI (Fig. 7C). The significant improvement in fiber size induced by SKM relative to saline ($P < 0.001$) and untreated SBI ($P < 0.05$) was sustained at this later time point.

SKM decreased PFMs' fibrotic response to birth injury compared with untreated SBI at 8 and 12 weeks after SBI (Fig. 7, D and E; $P = 0.01$), restoring intramuscular collagen content to the uninjured values (8 weeks $P = 0.8$; 12 weeks $P = 0.99$). Unexpectedly, saline also significantly decreased collagen accumulation at 8 weeks after injury relative to the untreated SBI group ($P = 0.006$). Similar to SKM, delayed saline injection resulted in an intramuscular collagen content indistinguishable from uninjured controls at 8 and 12 weeks after SBI ($P > 0.5$; Fig. 7, D and E).

For arteriole density, both SKM and saline administered at 4 weeks after SBI led to a decrease in the overall arteriole density (SBI + SKM and SBI + saline versus untreated SBI. $P = 0.002$; Fig. 7F) and of smaller arterioles (SBI + SKM and SBI + saline versus untreated SBI, $P < 0.0001$; Fig. 7G). The overall arteriole density did not differ significantly between the groups at 12 weeks after SBI (SBI + SKM versus SBI + saline, $P = 0.06$; versus untreated SBI, $P > 0.99$; versus uninjured controls, $P = 0.64$; and SBI + saline versus untreated SBI, $P = 0.18$; Fig. 7H), except for the increased vessel density after

saline injection compared with uninjured controls ($P = 0.004$). The density of smaller arterioles (Fig. 7I) decreased by 50% in the untreated SBI group at 12 weeks after injury compared with the 8-week time point, indicating some spontaneous recovery of the vascular component. Together, these results indicated that SKM administration 4 weeks after birth injury could mitigate PFM atrophy and fibrosis long term. On the other hand, saline injection is sufficient to reverse fibrosis.

We next analyzed acute and long-term transcriptional changes in PFMs in response to the delayed SKM injection using our custom Nanostring panel (table S2). Pubocaudalis was harvested at 3 and 7 days after injection (31 and 35 days after SBI, respectively), as well as at 8 weeks after injection (12 weeks after SBI) (Fig. 7A). Despite similar response to SKM and saline with respect to intramuscular collagen content, the principal components analysis revealed distinct clustering of SKM separate from saline and untreated SBI at early time points, whereas saline clustered together with untreated SBI (Fig. 7, J and K). At 8 weeks, the groups did not cluster separately (Fig. 7L), potentially because of the degradation of the hydrogel about 3 weeks after injection (19).

Gene expression profiles for each time point are summarized in figs. S11 to S13. Clustered heatmaps of the differentially expressed genes between SKM and saline representing fold change relative to untreated SBI are shown in Fig. 7 (M to O), with pairwise comparisons indicated in fig. S14. At the acute time points, SKM up-regulated genes related to the immune response: monocytes [*myeloid differentiation primary response 88* (*Myd88*)], macrophages [*adhesion g protein-coupled receptor e1* (*Adgre1*)], macrophages type 1 [*Nos2* and *signal transducer and activator of transcription 1* (*Stat1*)], macrophages type 2 [*Arg1* and *signal transducer and activator of transcription 6* (*Stat6*)], T cells [*natural killer cell granule protein 7* (*Nkg7*)], and T helper cells type 1 (*Tbx21*). We identified increased expression of genes associated with proinflammatory [*interleukin 12b* (*Il12b*), *Il1b, tumor necrosis factor* (*Tnf*), *Ccl2, Ccl3, chemokine (c-c motif) ligand 4* (*Ccl4*), *chemokine (c-c motif) receptor 2* (*Ccr2*), *chemokine (c-c motif) receptor 5* (*Ccr5*), *Cxcl1, chemokine (c-x-c motif) ligand 5* (*Cxcl5*), and *chemokine (c-x-c motif) receptor 2* (*Cxcr2*)] and proregenerative [*interleukin 10 receptor subunit alpha* (*Il10ra*), *interleukin* (*Il33*), and *insulin like growth factor 1* (*Igf1*)] mediators. For the myogenesis pathway, genes that aid in the activation [3 and 7 days, *hepatocyte growth factor* (*Hgf*)] and differentiation [7 days, *ADAM metallopeptidase domain 12* (*Adam12*)] of MuSCs and cellular survival [7 days, *hyaluronan synthase 1* (*Has1*), and *cellular communication network factor 4* (*Ccn4*)] were up-regulated. Genes associated with muscle structure were down-regulated [3 days, *troponin t1* (*Tnnt1*), *tropomyosin 3* (*Tpm3*), *titin-cap* (*Tcap*), *myosin light chain kinase 2* (*Mylk2*), *myosin binding protein c1* (*Mybpc1*), *myosin binding protein c2* (*Mybpc2*), *myosin heavy chain 1* (*Myh1*), *actin alpha 1* (*Acta1*), *actinin alpha 2* (*Actn2*), *myosin heavy chain 7* (*Myh7*), *troponin T3* (*Tnnt3*), *tropomyosin 4* (*Tpm4*), and *titin* (*Ttn*)]. Although upstream genes related to muscle anabolism [*activator protein 1* (*Junb*), *ribosomal protein s6 kinase a1* (*Rps6ka1*), and *follistatin* (*Fst*)] were up-regulated at 3 and 7 days, the downstream targets remained unchanged. For ECM remodeling, up-regulation of ECM-related genes was identified at both time points [*matrix metallopeptidase 2* (*Mmp2*), *matrix metallopeptidase 9* (*Mmp9*), *Timp1, Tgfb*, and *cellular communication network factor 2* (*Ccn2*)] with increased expression of collagens (*Col1a1* and *Col3a1*) at 7 days. For vascularization pathways,

although receptor genes related to vascularization were up-regulated [*Kdr*, *neuropilin 1* (*Nrp1*), and *tyrosine kinase with immunoglobulin like and egf like domains 1* (*Tie1*)], the ligands were not differentially expressed. Last, we observed an up-regulation of genes involved in the development [*agrin* (*Agrn*), *erb-b2 receptor tyrosine kinase 2* (*Erbb2*), *pleiotrophin* (*Ptn*), and *Tnc*] and maturation [*App* and *utrophin* (*Utrn*)] of neuromuscular junctions at 3 and 7 days. At 8 weeks after injection, we observed up-regulation of *Adgre1*, *Nkg7*, and *interferon regulatory factor 4* (*Irf4*) (immune response) and down-regulation of *matrix metallopeptidase 8* (*Mmp8*) (ECM remodeling) genes in the SKM group. Together, our findings indicated that administration of SKM 4 weeks after birth injury increased the expression of genes associated with the immune response, myogenesis, and ECM remodeling acutely after the injection, which affected the observed phenotype long-term. After hydrogel degradation (19), a limited number of genes continued to be differentially expressed in PFMs, with sustained effect on the histological parameters analyzed.

DISCUSSION

We demonstrate that the pubovisceralis exhibited atrophy and fibrosis in parous women with symptomatic POP. In the rat model of SBI, these pathological alterations followed transcriptomic changes, including the down-regulation of genes associated with anabolism and persistent up-regulation of ECM remodeling and inflammatory genes. Last, we showed that SKM can prevent, mitigate, or reverse these alterations caused by birth injury.

Clinical studies have identified that PFM injury is related to excessive strain during parturition, as opposed to compression or denervation (30). The resultant radiologically detected PFM avulsions are strongly associated with PFDs (31, 32). However, avulsion injury is not present in all women with decreased PFM strength. Furthermore, a proportion of PFM avulsions observed soon after childbirth are not evident 1 year postpartum (10), and a large-scale cadaveric investigation demonstrated absence of radiologically visualized "avulsions" on direct anatomic dissections (9). Together with our findings in the rat model (12), the above supports our notion that birth injury can lead to pathological transformations of PFMs not detectable by conventional imaging modalities. Our histological findings are consistent with the altered collagen content of other pelvic soft tissues, specifically vagina, in women with POP, presumed to be due to chronic inflammation (33, 34). Because causal experiments focused on deep pelvic structures such as PFMs are constrained in postpartum women, we relied on a preclinical model of SBI to investigate PFM response to strains associated with parturition.

The regeneration of limb muscles is mainly completed within a 4-week recovery period (14, 27). In contrast, we demonstrated that PFMs do not return to baseline after SBI, even in a highly regenerative rodent model. Multiple studies have concluded that acute injury is followed by a temporally regulated immune response that affects muscle repair (14, 35). The proinflammatory phase lasts up to 3 to 4 days after injury, followed by the proregenerative phase that promotes constructive remodeling. On the basis of our gene expression and flow cytometry analyses, the proinflammatory and proregenerative phases overlap during the acute period after SBI, with the inflammatory response sustained through 31 days

after injury. Overall, our data suggested that the inflammatory response of PFMs after SBI negatively affects pathways related to muscle growth, ECM remodeling, and vascularization.

Skeletal muscle growth occurs via myogenesis or through increase in protein synthesis. In our study, the up-regulation of proregenerative mediators correlates with the increased expression of genes associated with MuSC differentiation (fig. S15) and increased density of differentiated Myog[+] MuSCs (Fig. 3B). Consistently, the up-regulation of proinflammatory mediators coincided with the up-regulation of genes involved in MuSC expansion (fig. S15) and the increased density of Pax7^{+} MuSCs (Fig. 3C). Because myogenesis followed the expected time course (26), we focused on protein turn-over pathways to identify mechanisms responsible for PFM atrophy. The AkT/mTOR pathway, involved in protein synthesis, is negatively influenced by prolonged inflammation (36). Our data suggest that persistent inflammation after birth injury could be involved in the down-regulation of the AkT/mTOR pathway. The activation of this pathway involves phosphorylation of its components, which we did not assess in the study; however, the transcriptional, translational, and posttranslational alterations in this pathway are highly correlative during anabolism (37, 38).

After muscle injury, a temporal increase in ECM deposition is crucial for muscle repair. However, excessive ECM production and dysregulation of ECM metabolism lead to a pathological increase in ECM components, mainly collagen I (39). Although the up-regulation of genes associated with the temporal ECM deposition is expected, we suggest that the sustained expression of *Tgfb1*, a master regulator of fibrosis, and *Timp1*, an inhibitor of ECM degradation (39), leads to PFM fibrosis.

Inflammation has been shown to alter vascularization (25). Impaired recovery of smaller arterioles to baseline can affect oxygen and nutrient delivery to myofibers (14, 40). In our study, the sustained increase in smaller arterioles could be associated with the up-regulation of the indirect stimulators of arteriogenesis (*Ccl2*, *Tnfa*, and *Tgfb1*).

After characterizing PFMs' response to birth injury, we explored a therapeutic approach to potentiate constructive remodeling after SBI. Among regenerative strategies, cell-based therapies introduce challenges related to cell survival and engraftment, potential tumorigenicity, high costs, and short shelf life (41). In contrast, acellular low-cost immunomodulatory biomaterials can be used to potentiate endogenous regeneration (22, 42). Here, we investigated the administration of SKM at two translationally relevant time points. As a preventative measure, SKM could be used on labor and delivery units for women at high risk for PFM injury [operative vaginal delivery, prolonged second stage of labor, macrosomia, and obstetrical laceration (43)]. As a therapeutic intervention, SKM could be administered after clinically detected PFM weakness (44) at the postpartum visit, scheduled within 2 months after childbirth. A similar injectable ECM hydrogel derived from porcine myocardium was recently tested in phase 1 clinical trial in patients after myocardial infarction (45, 46), underscoring translational potential of this therapy.

Immediate delivery of SKM after SBI improved PFM phenotype. We opine that the increase in PFM fiber area is due to the material's enhancement of the expanding MuSC population,

as observed in a hindlimb ischemia model (19, 22). In addition, we suggest that SKM mitigates fibrosis by down-regulating ECM remodeling genes, such as *Ccn2*, involved in ECM deposition (39). Last, SKM mitigates the altered vascularization, potentially by down-regulating the inflammatory-related genes (*Ccl2*) (47).

In contrast to the immediate injection, delayed administration of SKM induced more differences in gene expression. The differential expression of genes related to the proinflammatory and proregenerative responses is consistent with the well-established immunomodulatory properties of ECM hydrogels (48) in a more stable tissue environment than that at the time of injury. Although delayed SKM injection did not up-regulate genes directly associated with MuSC function, SKM up-regulated genes that aid in myogenesis: *Hgf* and *Adam12*. The former is involved in the migration and activation of MuSCs (49), whereas the latter is expressed at the time of MuSC differentiation and fusion (50). Thus, biomaterial administration 4 weeks after SBI increases the PFM fiber size via its impact on myogenesis.

Although the gene expression profile after SKM or saline injection differs, the activity of saline may be a consequence of the inflammation and subsequent wound healing response to the micro-injury associated with the process of injecting tissue (51). Even though improvements in the histological parameters were observed at 4 and 8 weeks after injection, the effects of SKM were more prominent at 4 weeks. The above may in part be due to the long-term spontaneous recovery after birth injury, owing to the highly regenerative capacity of a rodent model (52).

One of the limitations of our study is that we used a biased approach to assess transcriptional changes, which limits discovery and in-depth analysis of pathway regulation after SBI and biomaterial injection. Another limitation is related to testing mechanical properties of PFMs. Existing protocols for appendicular muscles are not applicable given that PFMs do not have tendons at the origin. Therefore, a customized mechanical rig is necessary to assess muscle function, which we are exploring for future studies. In addition, we performed our studies in a nonpregnant model. This was important to obviate potential confounding effects of the complex hormonal milieu associated with pregnancy, size and number of pups, and the effects of spontaneous parturition. Sexually mature young animals were chosen because we focused on interventions around the time of birth injury. Using older animals to account for increasing maternal age is another avenue for future investigations.

In conclusion, our study demonstrated that PFMs of parous women with symptomatic PFDs exhibit atrophy and fibrosis. In addition, we showed that the rat SBI model recapitulates this phenotype. Last, we provide studies in a continuum of investigations focused on the use of minimally invasive acellular biomaterials to prevent or mitigate pathological alterations of PFMs consequent to birth injury.

MATERIALS AND METHODS

Study design

The objectives of this study were to (i) compare PFM morphological properties in parous women with symptomatic POP and age-comparable nulliparous and parous cadaveric donors without history of PFDs; (ii) investigate PFMs' response to birth injury along the biologically relevant continuum using a validated preclinical model of SBI; and (iii) investigate the efficacy of SKM at two translationally relevant time points after birth injury. Animals were euthanized at acute, subacute, and long-term time points after SBI. Histological, immunohistochemical, gene expression, and flow cytometry analyses were used to investigate PFM response to birth injury. The sample size, indicated in the figure legends, was calculated a priori (see Statistical analysis). For human samples, the inclusion/exclusion criteria are indicated below. Animals were randomized for the biomaterial-related studies. Each study was performed once, data include biological replicates, outliers were not excluded; the quantitative analyses were conducted by the investigators blinded to the group identity.

PFM collection from women with POP

The pubovisceralis biopsies were obtained during surgical repair of POP ($n = 20$). Participants were enrolled in the institutional review board–approved study at two sites, Kaiser Permanente San Diego and the University of California San Diego (reference numbers: 6378 and 111845). Relevant obstetrical, surgical, and medical histories were collected from the electronic medical records. Immediately after procurement, muscle biopsies were pinned to a cork at slack length, snap-frozen in isopentane chilled with liquid nitrogen, transported on dry ice, and stored at −80°C. At the time of tissue processing, muscle biopsies were embedded in optimal cutting temperature material (OCT) for cryosectioning and snap-frozen again. Ten-micrometer-thick cross sections were stained with hematoxylin and eosin (H&E) for myofibrillar shape and packing; oil-red-o for intramuscular fat content; and Gomori's trichrome for collagen content, fiber area, and centralized nuclei, using well-established methods.

Cadaveric PFM collection

Nulliparous ($n = 4$) and parous ($n = 7$) cadaveric donors without history of PFDs were used as controls. Samples were obtained through the Bequest Body Donation Program at the University of Minnesota, which provides relevant obstetrical, surgical, and medical history for each donor. Donors with a history of gynecologic or colorectal malignancy, pelvic metastasis, pelvic radiation, connective tissue disorder, myopathy, rectal prolapse, colectomy, or proctectomy were excluded. Biopsies of pubovisceralis were obtained within 7 days postmortem and immediately processed as described above.

SBI rat model

All procedures were approved by the Institutional Animal Care and Use Committee at the University of California, San Diego (reference number: S13008). Vaginal distention was performed using an established protocol (12) in 3-month-old Sprague-Dawley female rats

(Envigo) anesthetized with 2.5% isoflurane + oxygen for the duration of the procedure. Briefly, a 12-French transurethral catheter (Bard Medical) with the tip cut off was inserted into the vagina with a 130-g weight attached to the end of the catheter. The balloon was inflated to 5 ml and left in place for 2 hours, after which it was pulled through the introitus to replicate circumferential and downward strains associated with parturition. Although the magnitude of strain can be varied using different distention volumes (12, 53), 5 ml was chosen to induce sarcomere hyperelongation associated with myofibrillar disruption, the primary mechanism of mechanical muscle injury, on the basis of our previous studies (12, 53).

Rat PFM collection to assess endogenous response to SBI

Animals were euthanized, and the pubocaudalis muscle was harvested at 4, 8, or 12 weeks after SBI. To assess early response to SBI, the pubocaudalis was also harvested at 1, 3, 7, or 10 days after injury to assess the overall tissue morphology by H&E and to quantify the differentiation and self-renewal phases of MuSCs by immunohistochemistry. Harvested muscles were embedded in OCT and snap-frozen in isopentane chilled with liquid nitrogen. In addition, the pubocaudalis was harvested at 1, 3, 7, 10, 31, and 35 days after SBI to assess the expression of genes relevant to muscle regeneration using Nanostring. Muscles were submerged in RNAlater, stored at 4°C overnight, and transferred to −80°C before RNA isolation. For flow cytometry analysis, pubocaudalis was harvested at 3, 7, 10, and 31 days after SBI. Muscles were immediately submerged in media and processed for cell isolation and antibody incubation to identify immune cellular populations (see Supplementary Materials and Methods).

Biomaterial injection and analyses of treated PFMs

Because the ECM composition between porcine longissimus dorsi muscle and porcine PFMs is overall similar (fig. S16), the SKM was fabricated from longissimus dorsi muscle. The relatively small size of the porcine PFMs would lead to substantially more costly and laborious hydrogel development. SKM was fabricated and characterized as described in Supplementary Materials and Methods (figs. S17 and S18 and table S10).

For the immediate injection, rats were subjected to SBI, followed by 10-μl saline (experimental control) or SKM injection into the rostral portion of the pubocaudalis via transobturator approach (fig. S19A) with a 30-gauge needle on a Hamilton syringe. For the delayed injection, either saline or SKM was injected 4 weeks after SBI. To assure reliable SKM injection, we first performed multiple injections with biomaterial prelabeled with India ink or Alexa Fluor 568 (fig. S19, B and C). Efficacy of the biomaterial treatment was assessed by histological analysis and gene expression studies (see Supplementary Materials and Methods).

Statistical analysis

Sample size for histological analysis was determined on the basis of a previous SKM study (22). Using G*power software, six animals per group per time point were needed to achieve 90% power at a significance of 0.05 with two-sided testing. For the gene expression studies, preliminary quantitative reverse transcription polymerase chain reaction data were used to

calculate sample size. Ten animals per group per time point were needed to achieve 80% power at a significance set to 0.05 with two-sided testing. Parametric data (table S11) were compared using Student's *t* test; or one- or two-way analysis of variance (ANOVA) followed by Tukey's or Šidák post hoc pairwise comparisons, respectively. Nonparametrically distributed fiber area data were analyzed by Mann-Whitney or Kruskal-Wallis test followed by Dunn's pairwise comparisons (54, 55). Data, presented as mean ± SEM or median (interquartile range), were analyzed using GraphPad Prism v8.0. NanoStringDiff package in R was used for gene expression normalization and differential expression analysis, with significance set to 0.05 and a fold change cutoff of 1 ± 0.25 (56).

Supplementary Material

Refer to Web version on PubMed Central for supplementary material.

Acknowledgments:

Data and materials availability:

All data associated with this study are available in the main text or the Supplementary Materials. Nanostring data are available from the NCBI GEO database with the accession number GSE237062.

REFERENCES AND NOTES

1. Shen L, Yang J, Bai X, Sun Z, Analysis of the current status of pelvic floor dysfunction in urban women in Xi'an City. Ann. Palliat. Med. 9, 979–984 (2020). [PubMed: 32434360]

2. Wu JM, Vaughan CP, Goode PS, Redden DT, Burgio KL, Richter HE, Markland AD, Prevalence and trends of symptomatic pelvic floor disorders in U.S. women. Obstet. Gynecol. 123, 141–148 (2014). [PubMed: 24463674]

3. Zeleke BM, Bell RJ, Billah B, Davis SR, Symptomatic pelvic floor disorders in community-dwelling older Australian women. Maturitas 85, 34–41 (2016). [PubMed: 26857877]

4. Hasuda T, Ueda A, Wei C-N, Prevalence of symptomatic pelvic floor disorders among Japanese women. J. Women's Health Care 6, 4 (2017).

5. Blomquist JL, Carroll M, Munoz A, Handa VL, Pelvic floor muscle strength and the incidence of pelvic floor disorders after vaginal and cesarean delivery. Am. J. Obstet. Gynecol. 222, 62.e1–62.e8 (2020).

6. Hallock JL, Handa VL, The Epidemiology of pelvic floor disorders and childbirth: An update. Obstet. Gynecol. Clin. North Am. 43, 1–13 (2016). [PubMed: 26880504]

7. Brooks SV, Zerba E, Faulkner JA, Injury to muscle fibres after single stretches of passive and maximally stimulated muscles in mice. J. Physiol. 488, 459–469 (1995). [PubMed: 8568684]

8. Jing D, Ashton-Miller JA, DeLancey JOL, A subject-specific anisotropic visco-hyperelastic finite element model of female pelvic floor stress and strain during the second stage of labor. J. Biomech. 45, 455–460 (2012). [PubMed: 22209507]

9. Da Silva AS, Digesu GA, Dell'Utri C, Fritsch H, Piffarotti P, Khullar V, Do ultrasound findings of levator ani "avulsion" correlate with anatomical findings: A multicenter cadaveric study. Neurourol.Urodyn. 35, 683–688 (2016). [PubMed: 25982354]

10. van Delft KWM, Thakar R, Sultan AH, IntHout J, Kluivers KB, The natural history of levator avulsion one year following childbirth: A prospective study. BJOG 122, 1266–1273 (2015). [PubMed: 25514994]

11. Alperin M, Tuttle LJ, Conner BR, Dixon DM, Mathewson MA, Ward SR, Lieber RL, Comparison of pelvic muscle architecture between humans and commonly used laboratory species. Int. Urogynecol. J. 25, 1507–1515 (2014). [PubMed: 24915840]

12. Catanzarite T, Bremner S, Barlow CL, Bou-Malham L, O'Connor S, Alperin M, Pelvic muscles' mechanical response to strains in the absence and presence of pregnancy-induced adaptations in a rat model. Am. J. Obstet. Gynecol. 218, 512.e1–512.e9 (2018).

13. Lieber RL, Fridén J, Mechanisms of muscle injury gleaned from animal models. Am. J. Phys. Med. Rehabil. 81, S70–S79 (2002). [PubMed: 12409812]

14. Hardy D, Besnard A, Latil M, Jouvion G, Briand D, Thepenier C, Pascal Q, Guguin A, Gayraud-Morel B, Cavaillon JM, Tajbakhsh S, Rocheteau P, Chretien F, Comparative study of injury models for studying muscle regeneration in mice. PLOS ONE 11, e0147198 (2016). [PubMed: 26807982]

15. Wallace SL, Miller LD, Mishra K, Pelvic floor physical therapy in the treatment of pelvic floor dysfunction in women. Curr. Opin. Obstet. Gynecol. 31, 485–493 (2019). [PubMed: 31609735]

16. Gormley EA, Evaluation and management of the patient with a failed midurethral synthetic sling. Can. Urol. Assoc. J. 6, S123–S124 (2012). [PubMed: 23092772]

17. George AT, Kalmar K, Panarese A, Dudding TC, Nicholls RJ, Vaizey CJ, Long-term outcomes of sacral nerve stimulation for fecal incontinence. Dis. Colon Rectum 55, 302–306 (2012). [PubMed: 22469797]

18. Sandall J, Tribe RM, Avery L, Mola G, Visser GHA, Homer CSE, Gibbons D, Kelly NM, Kennedy HP, Kidanto H, Taylor P, Temmerman M, Short-term and long-term effects of caesarean section on the health of women and children. Lancet 392, 1349–1357 (2018). [PubMed: 30322585]

19. DeQuach JA, Lin JE, Cam C, Hu D, Salvatore MA, Sheikh F, Christman KL, Injectable skeletal muscle matrix hydrogel promotes neovascularization and muscle cell infiltration in a hindlimb ischemia model. Eur. Cell. Mater. 23, 400–412 (2012). [PubMed: 22665162]

20. Zhang D, Zhang Y, Zhang Y, Yi H, Wang Z, Wu R, He D, Wei G, Wei S, Hu Y, Deng J, Criswell T, Yoo J, Zhou Y, Atala A, (*) Tissue-specific extracellular matrix enhances skeletal muscle precursor cell expansion and differentiation for potential application in cell therapy. Tissue Eng. Part A 23, 784–794 (2017). [PubMed: 28463580]

21. Rao N, Agmon G, Tierney MT, Ungerleider JL, Braden RL, Sacco A, Christman KL, Engineering an injectable muscle-specific microenvironment for improved cell delivery using a nanofibrous extracellular matrix hydrogel. ACS Nano 11, 3851–3859 (2017). [PubMed: 28323411]

22. Ungerleider JL, Johnson TD, Hernandez MJ, Elhag DI, Braden RL, Dzieciatkowska M, Osborn KG, Hansen KC, Mahmud E, Christman KL, Extracellular matrix hydrogel promotes tissue remodeling, arteriogenesis, and perfusion in a rat hindlimb ischemia model. JACC Basic Transl. Sci. 1, 32–44 (2016). [PubMed: 27104218]

23. Cheng YW, Caughey AB, Second stage of labor. Clin. Obstet. Gynecol. 58, 227–240 (2015). [PubMed: 25851851]

24. Ranjbar K, Rahmani-Nia F, Shahabpour E, Aerobic training and l-arginine supplementation promotes rat heart and hindleg muscles arteriogenesis after myocardial infarction. J. Physiol. Biochem. 72, 393–404 (2016). [PubMed: 27121159]

25. Gibbons MC, Singh A, Anakwenze O, Cheng T, Pomerantz M, Schenk S, Engler AJ, Ward SR, Histological evidence of muscle degeneration in advanced human rotator cuff disease. J. Bone Joint Surg. Am. 99, 190–199 (2017). [PubMed: 28145949]

26. Rantanen J, Hurme T, Lukka R, Heino J, Kalimo H, Satellite cell proliferation and the expression of myogenin and desmin in regenerating skeletal muscle: Evidence for two different populations of satellite cells. Lab. Invest. 72, 341–347 (1995). [PubMed: 7898053]

27. Cutler AA, Pawlikowski B, Wheeler JR, Dalla Betta N, Elston T, O'Rourke R, Jones K, Olwin BB, The regenerating skeletal muscle niche drives satellite cell return to quiescence. iScience 25, 104444 (2022). [PubMed: 35733848]

28. Rigamonti E, Touvier T, Clementi E, Manfredi AA, Brunelli S, Rovere-Querini P, Requirement of inducible nitric oxide synthase for skeletal muscle regeneration after acute damage. J. Immunol. 190, 1767–1777 (2013). [PubMed: 23335752]

29. Zhu J, Paul WE, Peripheral CD4+ T-cell differentiation regulated by networks of cytokines and transcription factors. Immunol. Rev. 238, 247–262 (2010). [PubMed: 20969597]

30. Ashton-Miller JA, DeLancey JOL, Mechanisms of Pelvic Floor Trauma During Vaginal Delivery. Springer, (2021).

31. DeLancey JOL, Kearney R, Chou Q, Speights S, Binno S, The appearance of levator ani muscle abnormalities in magnetic resonance images after vaginal delivery. Obstet. Gynecol. 101, 46–53 (2003). [PubMed: 12517644]

32. Cassado J, Simo M, Rodriguez N, Porta O, Huguet E, Mora I, Girvent M, Fernandez R, Gich I, Prevalence of levator ani avulsion in a multicenter study (PAMELA study). Arch. Gynecol. Obstet. 302, 273–280 (2020). [PubMed: 32449062]

33. Li Y, Zhang QY, Sun BF, Ma Y, Zhang Y, Wang M, Ma C, Shi H, Sun Z, Chen J, Yang YG, Zhu L, Single-cell transcriptome profiling of the vaginal wall in women with severe anterior vaginal prolapse. Nat. Commun. 12, 87 (2021). [PubMed: 33397933]

34. Gong R, Xia Z, Collagen changes in pelvic support tissues in women with pelvic organ prolapse. Eur. J. Obstet. Gynecol. Reprod. Biol. 234, 185–189 (2019). [PubMed: 30710765]

35. Tidball JG, Regulation of muscle growth and regeneration by the immune system. Nat. Rev. Immunol. 17, 165–178 (2017). [PubMed: 28163303]

36. Costamagna D, Costelli P, Sampaolesi M, Penna F, Role of inflammation in muscle homeostasis and myogenesis. Mediators Inflamm. 2015, 805172 (2015). [PubMed: 26508819]

37. Morissette MR, Cook SA, Buranasombati C, Rosenberg MA, Rosenzweig A, Myostatin inhibits IGF-I-induced myotube hypertrophy through Akt. Am. J. Physiol. Cell Physiol. 297, C1124–C1132 (2009). [PubMed: 19759331]

38. Boudra R, Lagrafeuille R, Lours-Calet C, de Joussineau C, Loubeau-Legros G, Chaveroux C, Saru JP, Baron S, Morel L, Beaudoin C, mTOR transcriptionally and post-transcriptionally regulates Npm1 gene expression to contribute to enhanced proliferation in cells with Pten inactivation. Cell Cycle 15, 1352–1362 (2016). [PubMed: 27050906]

39. Gillies AR, Lieber RL, Structure and function of the skeletal muscle extracellular matrix. Muscle Nerve 44, 318–331 (2011). [PubMed: 21949456]

40. Fernando CA, Pangan AM, Cornelison D, Segal SS, Recovery of blood flow regulation in microvascular resistance networks during regeneration of mouse gluteus maximus muscle. J. Physiol. 597, 1401–1417 (2019). [PubMed: 30575953]

41. Dodson BP, Levine AD, Challenges in the translation and commercialization of cell therapies. BMC Biotechnol. 15, 70 (2015). [PubMed: 26250902]

42. Christman KL, Biomaterials for tissue repair. Science 363, 340–341 (2019). [PubMed: 30679357]

43. Friedman S, Blomquist JL, Nugent JM, McDermott KC, Muñoz A, Handa VL, Pelvic muscle strength after childbirth. Obstet. Gynecol. 120, 1021–1028 (2012). [PubMed: 23090518]

44. Frawley HC, Galea MP, Phillips BA, Sherburn M, Bo K, Reliability of pelvic floor muscle strength assessment using different test positions and tools. Neurourol.Urodyn. 25, 236–242 (2006). [PubMed: 16299815]

45. Seif-Naraghi SB, Singelyn JM, Salvatore MA, Osborn KG, Wang JJ, Sampat U, Kwan OL, Strachan GM, Wong J, Schup-Magoffin PJ, Braden RL, Bartels K, DeQuach JA, Preul M, Kinsey AM, DeMaria AN, Dib N, Christman KL, Safety and efficacy of an injectable extracellular matrix hydrogel for treating myocardial infarction. Sci. Transl. Med. 5, 173ra125 (2013).

46. Traverse JH, Henry TD, Dib N, Patel AN, Pepine C, Schaer GL, DeQuach JA, Kinsey AM, Chamberlin P, Christman KL, First-in-man study of a cardiac extracellular matrix hydrogel in early

and late myocardial infarction patients. JACC Basic Transl. Sci. 4, 659–669 (2019). [PubMed: 31709316]

47. Carmeliet P, Mechanisms of angiogenesis and arteriogenesis. Nat. Med. 6, 389–395 (2000). [PubMed: 10742145]

48. Dziki JL, Huleihel L, Scarritt ME, Badylak SF, Extracellular matrix bioscaffolds as immunomodulatory biomaterials. Tissue Eng. Part A 23, 1152–1159 (2017). [PubMed: 28457179]

49. Dhawan J, Rando TA, Stem cells in postnatal myogenesis: Molecular mechanisms of satellite cell quiescence, activation and replenishment. Trends Cell Biol. 15, 666–673 (2005). [PubMed: 16243526]

50. Galliano MF, Huet C, Frygelius J, Polgren A, Wewer UM, Engvall E, Binding of ADAM12, a marker of skeletal muscle regeneration, to the muscle-specific actin-binding protein, α-actinin-2, is required for myoblast fusion. J. Biol. Chem. 275, 13933–13939 (2000). [PubMed: 10788519]

51. Thuilliez C, Dorso L, Howroyd P, Gould S, Chanut F, Burnett R, Histopathological lesions following intramuscular administration of saline in laboratory rodents and rabbits. Exp. Toxicol. Pathol. 61, 13–21 (2009). [PubMed: 18835765]

52. Khyeam S, Lee S, Huang GN, Genetic, epigenetic, and post-transcriptional basis of divergent tissue regenerative capacities among vertebrates. Adv. Genet. (Hoboken) 2, e10042 (2021). [PubMed: 34423307]

53. Rieger MM, Wong M, Burnett LA, Sesillo FB, Baynes BB, Alperin M, Mechanisms governing protective pregnancy-induced adaptations of the pelvic floor muscles in the rat preclinical model. Am. J. Obstet. Gynecol. 226, 708.e1–708.e13 (2022).

54. Baghdadi MB, Castel D, Machado L, Fukada SI, Birk DE, Relaix F, Tajbakhsh S, Mourikis P, Reciprocal signalling by Notch-collagen V-CALCR retains muscle stem cells in their niche. Nature 557, 714–718 (2018). [PubMed: 29795344]

55. Sun X, Wu J, Qiang B, Romagnuolo R, Gagliardi M, Keller G, Laflamme MA, Li R-K, Nunes SS, Transplanted microvessels improve pluripotent stem cell–derived cardiomyocyte engraftment and cardiac function after infarction in rats. Sci. Transl. Med. 12, eaax2992 (2020). [PubMed: 32967972]

56. Raman AT, Pohodich AE, Wan YW, Yalamanchili HK, Lowry WE, Zoghbi HY, Liu Z, Apparent bias toward long gene misregulation in MeCP2 syndromes disappears after controlling for baseline variations. Nat. Commun. 9, 3225 (2018). [PubMed: 30104565]

57. Phillips DIW, Caddy S, Ilic V, Fielding BA, Frayn KN, Borthwick AC, Taylor R, Intramuscular triglyceride and muscle insulin sensitivity: Evidence for a relationship in nondiabetic subjects. Metabolism 45, 947–950 (1996). [PubMed: 8769349]

58. Spang MT, Middleton R, Diaz M, Hunter J, Mesfin J, Banka A, Sullivan H, Wang R, Lazerson TS, Bhatia S, Corbitt J, D'Elia G, Sandoval-Gomez G, Kandell R, Vratsanos MA, Gnanasekaran K, Kato T, Igata S, Luo C, Osborn KG, Gianneschi NC, Eniola-Adefeso O, Cabrales P, Kwon EJ, Contijoch F, Reeves RR, DeMaria AN, Christman KL, Intravascularly infused extracellular matrix as a biomaterial for targeting and treating inflamed tissues. Nat. Biomed. Eng. 7, 94–109 (2023). [PubMed: 36581694]

59. Wisniewski JR, Zougman A, Nagaraj N, Mann M, Universal sample preparation method for proteome analysis. Nat. Methods 6, 359–362 (2009). [PubMed: 19377485]

60. Kong AT, Leprevost FV, Avtonomov DM, Mellacheruvu D, Nesvizhskii AI, MSFragger: Ultrafast and comprehensive peptide identification in mass spectrometry-based proteomics. Nat. Methods 14, 513–520 (2017). [PubMed: 28394336]

61. Hernandez MJ, Yakutis GE, Zelus EI, Hill RC, Dzieciatkowska M, Hansen KC, Christman KL, Manufacturing considerations for producing and assessing decellularized extracellular matrix hydrogels. Methods 171, 20–27 (2019). [PubMed: 31546012]

62. McCabe MC, Schmitt LR, Hill RC, Dzieciatkowska M, Maslanka M, Daamen WF, van Kuppevelt TH, Hof DJ, Hansen KC, Evaluation and refinement of sample preparation methods for extracellular matrix proteome coverage. Mol. Cell. Proteomics 20, 100079 (2021). [PubMed: 33845168]

63. Hill RC, Calle EA, Dzieciatkowska M, Niklason LE, Hansen KC, Quantification of extracellular matrix proteins from a rat lung scaffold to provide a molecular readout for tissue engineering. Mol. Cell. Proteomics 14, 961–973 (2015). [PubMed: 25660013]
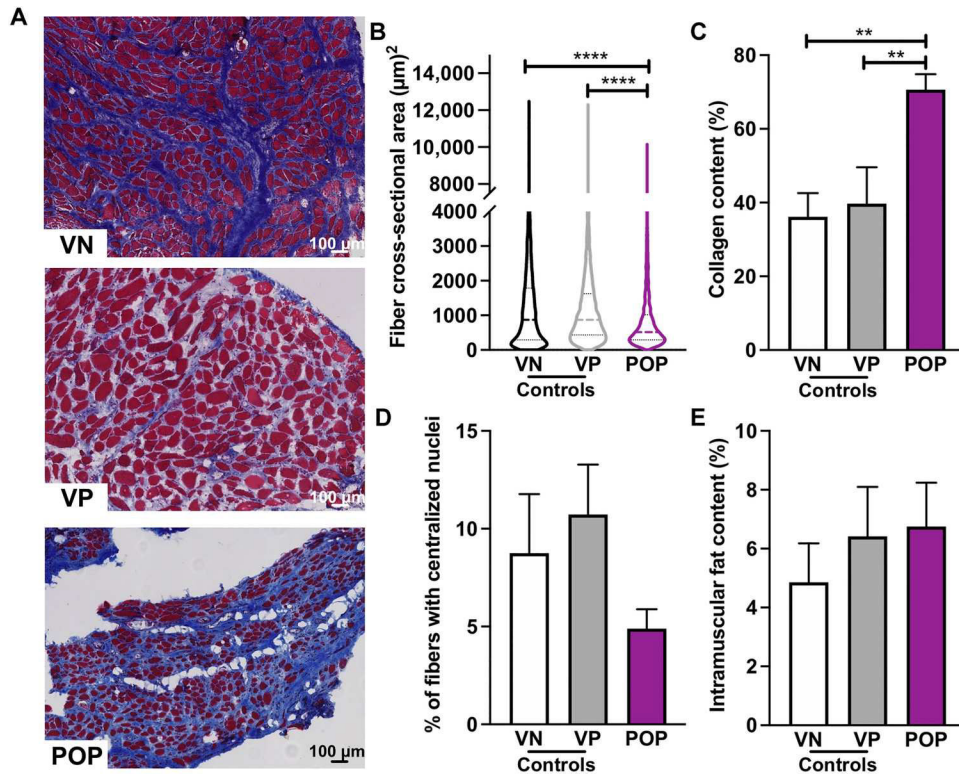
Fig. 1. PFMs in women with symptomatic pelvic floor disorders demonstrate an atrophic and fibrotic phenotype.

(**A**) Gomori'strichrome–stained (blue, intramuscular collagen content; red, muscle fibers) biopsy crosssections of the pubovisceralis portion of the levator ani muscle procured from VN and VP cadaveric donors without history of pelvic floor disorders and from parous women with POP. (**B**) Violin plots of fiber cross-sectional area. Shape of the plots demonstrates the distribution of the myofibers of varioussizes with a median indicated by the dash line. (**C**) Collagen content. (**D**) Centralized nuclei quantification. (**E**) Intramuscular fat content. $n = 4$ (VN); $n = 7$ (VP); $n = 20$ (POP) biological replicates. P values derived from one-way ANOVA followed by pairwise comparisons with Tukey's range test for parametric and Kruskal-Wallis followed by pairwise comparisons with Dunn's test for nonparametric data. $**P < 0.01$ and $****P < 0.0001$; mean ± SEM, median (interquartile range); scale bars, 100 μm.
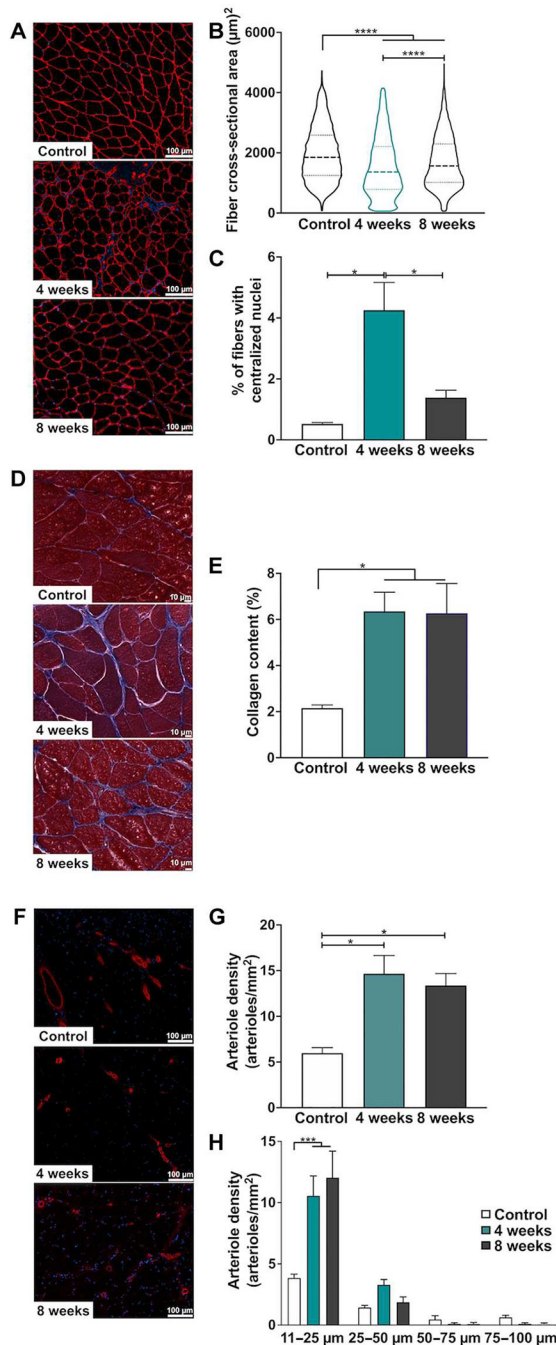
Fig. 2. Rat model of SBI recapitulating atrophic and fibrotic PFM phenotype observed in parous women with symptomatic PFDs.

(**A**) Laminin (red)– and nuclei (blue)–stained cross sections of the pubocaudalis portion of the levator ani muscle in uninjured controls, and 4 and 8 weeks after SBI groups, used for fiber cross-sectional area (**B**) and centralized nuclei (**C**) quantification; scale bars, 100 μm. (**D**) Masson's trichrome staining of pubocaudalis used for intramuscular collagen quantification (blue) (**E**); scale bars, 10 μm. (**F**) α–smooth muscle actin staining (red, arterioles; blue, nuclei) of the pubocaudalis, used for quantification of the total vessel

(arteriole) density (**G**) and distribution of vessels by size (**H**); scale bars, 100 μm. $n = 3$ to 6 per group biological replicates. *P* values derived from one- or two-way ANOVA followed by pairwise comparisons with Tukey's or Šidák range test, respectively, for parametric data and Kruskal-Wallis followed by pairwise comparisons with Dunn's test for nonparametrically distributed data. $*P < 0.05$, $***P < 0.001$, and $****P < 0.0001$; mean ± SEM, median (interquartile range).
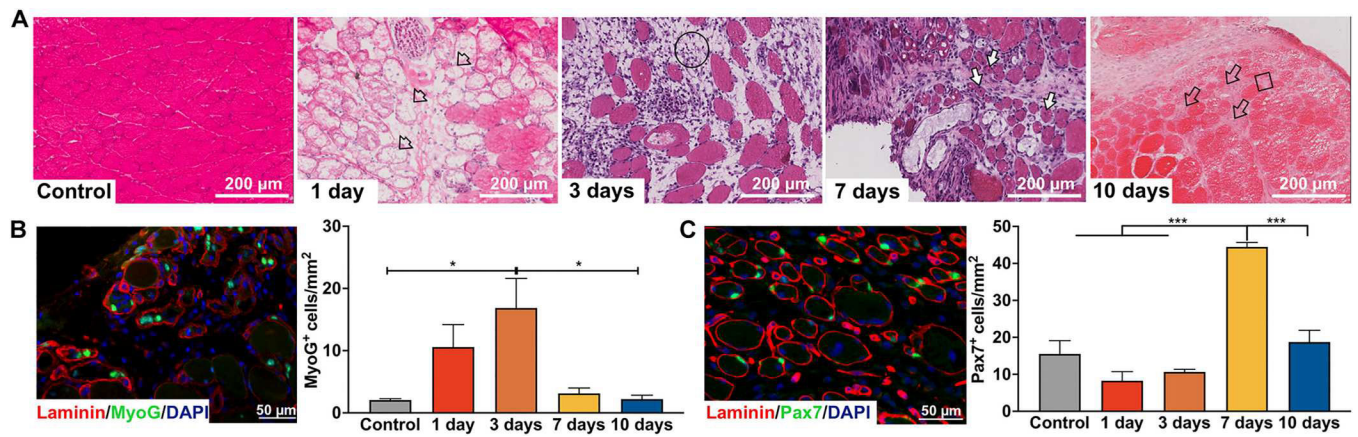
Fig. 3. Myogenesis of the pelvic floor muscles takes place within 1 week after SBI.
(**A**) H&E staining of pubocaudalis cross sections along a 10-day continuum after SBI; scale bars, 200 μm (basal lamina, arrowheads; cellular infiltration, circle and unfilled arrows; centralized nuclei, white arrows; endomysium, square). Muscle cross sections were incubated with antimyogenin antibodies for in situ quantification of differentiated MuSCs and assessment of muscle stem pool, respectively; laminin (red), DAPI (blue); scale bars, 50 μm. $n = 2$ or 3 per group biological replicates. P values derived from one-way ANOVA followed by pairwise comparisons with Tukey's range test. *$P < 0.05$ and ***$P < 0.001$; mean ± SEM.
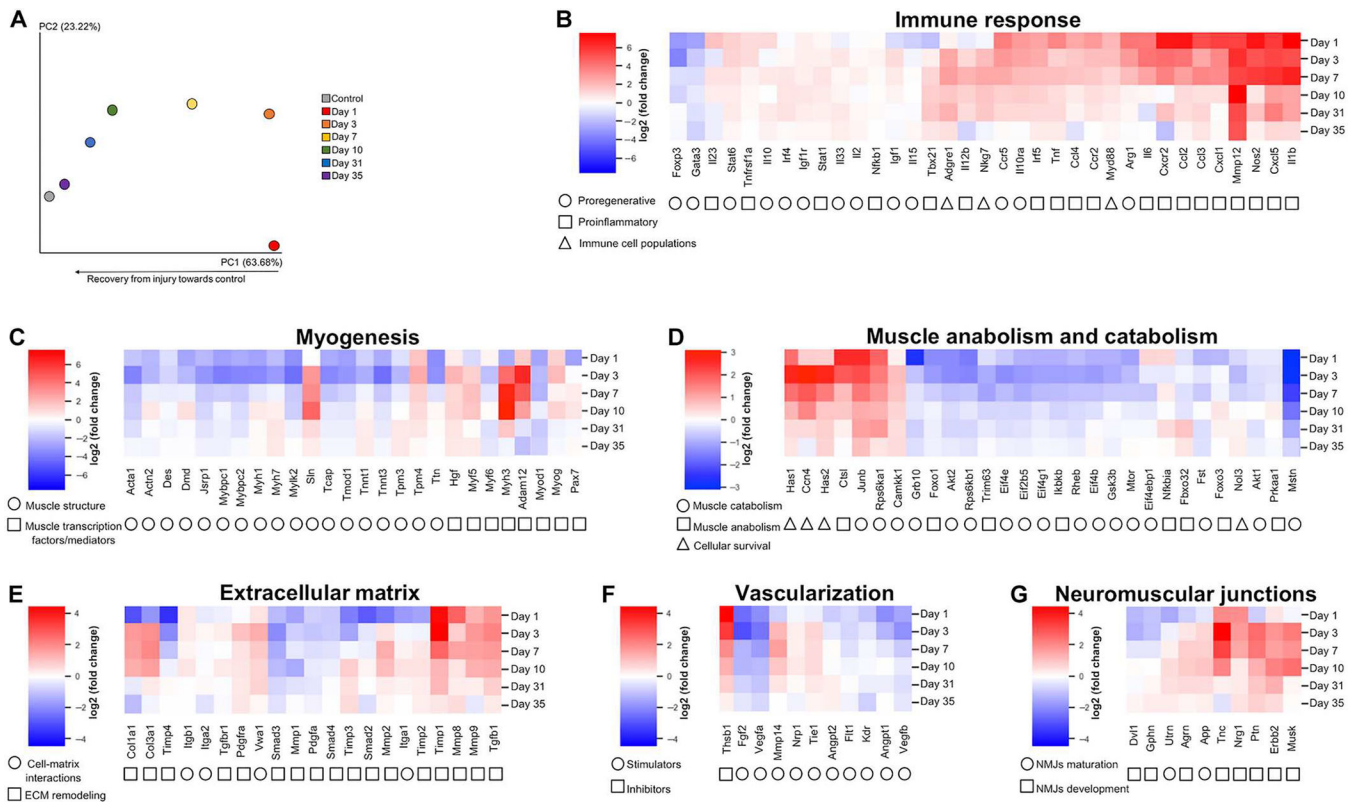
Fig. 4. SBI leads to sustained inflammatory response, up-regulation of ECM remodeling genes, and down-regulation of genes involved in muscle anabolism.
(**A**) Transcriptional signatures of the PFMs of the rat across different pathways were derived from the customized Nanostring nCounter panel with 150 genes. Principal components (PC) analysis includes gene expression in uninjured controls and at multiple time points during active muscle regeneration after SBI. (B to G) Unsupervised clustered heatmaps of fold changes at each time point with respect to control. Pathways examined include immune response (**B**), myogenesis (**C**), muscle anabolism and catabolism (**D**), extracellular matrix (**E**), vascularization (**F**), and neuromuscular junctions (**G**). $n = 3$ to 6 per group biological replicates. Gene expression analysis was analyzed on the basis of NanoStringDiff package in R.
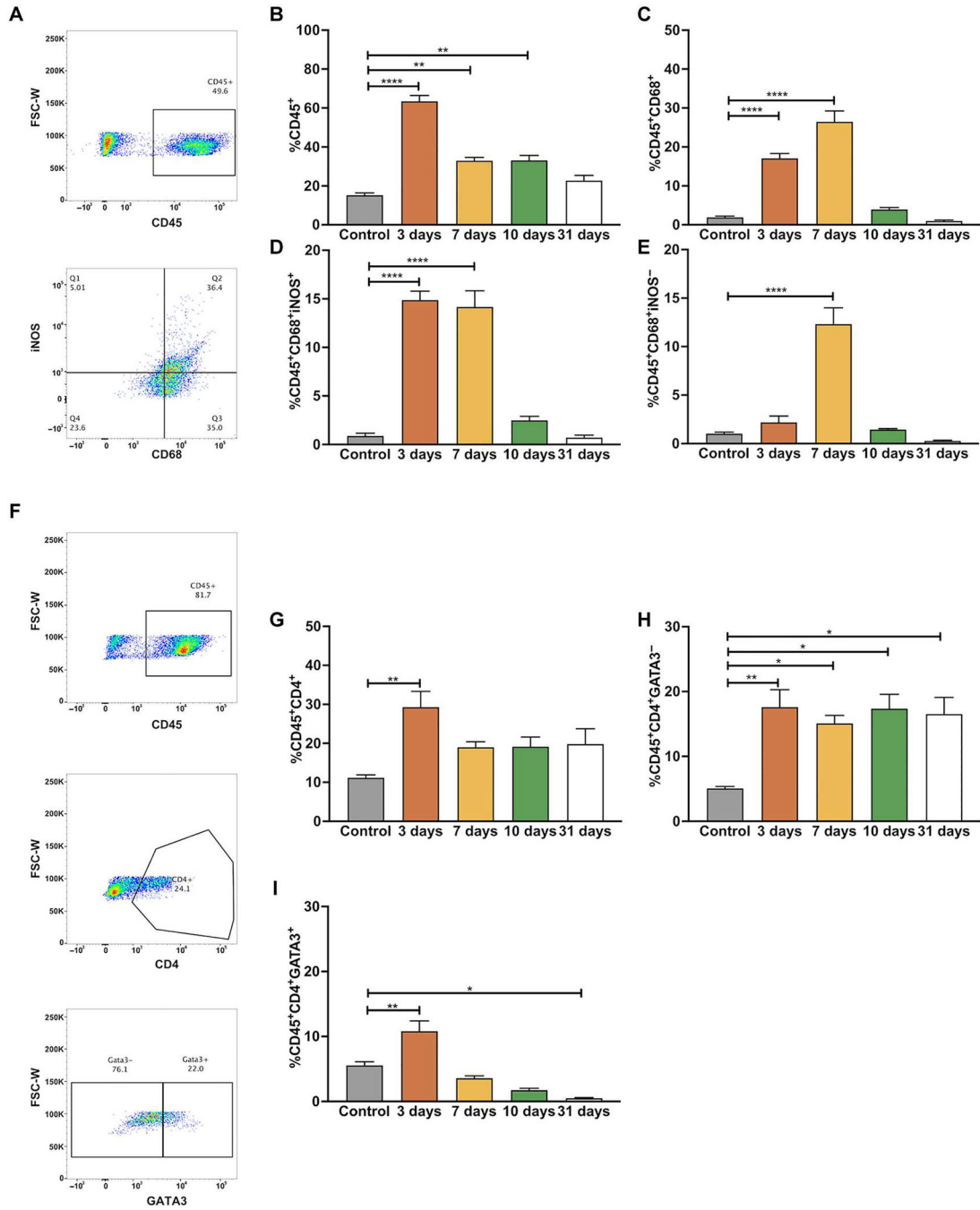
Fig. 5. Immune cellular dynamics indicate an increase of macrophages within a week after SBI with long-term increase of a CD45+CD4+GATA3− subpopulation of T helper cells. (**A**) Representative plots for macrophage populations showing percentage of CD45+, CD45+CD68−iNOS+ (Q1), CD45+CD68+iNOS+ (Q2), CD45+CD68+ iNOS− (Q3), and CD45+CD68−iNOS− (Q4) cells. Percentage of CD45+ (**B**), CD45+CD68+ (**C**), CD45+CD68+iNOS+ (**D**), and CD45+CD68+iNOS− (**E**) cells. (**F**) Representative plots of T helper cellular populations showing expression of CD45+, CD45+CD4+, CD45+CD4+GATA3−, and CD45+CD4+GATA3+ cells. Percentage of CD45+CD4+ (**G**),

CD45$^+$ CD4$^+$GATA3$^-$ (**H**), and CD45$^+$CD4$^+$GATA3$^+$ (**I**) cells. n = 3 to 6 per group biological replicates. P values derived from one-way ANOVA followed by pairwise comparisons with Dunnett's range test. *$P <$ 0.05, **$P <$ 0.01, and ****$P <$ 0.0001; mean $\pm$ SEM.
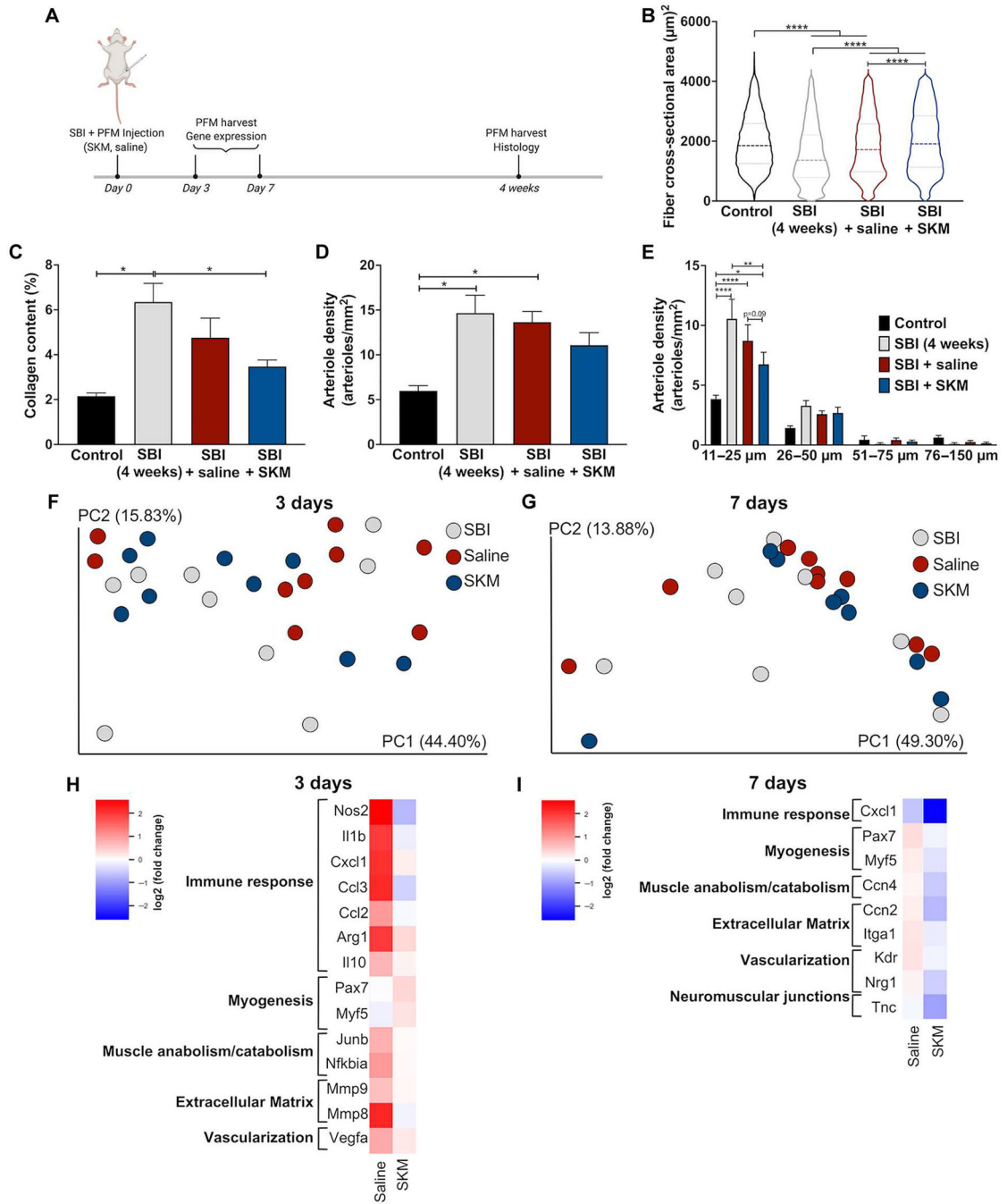
Fig. 6. Injection of SKM at the time of SBI prevents PFM atrophy and mitigates fibrosis.
(**A**) Study timeline. Pubocaudalis muscles of uninjured controls and animals subjected to
SBI, SBI + saline injection, or SBI + SKM injection were compared with respect to fiber
cross-sectional area (**B**); collagen content (**C**); overall vessel (arteriole) density (**D**); and
vessel (arteriole) density separated by size (**E**). PC analysis of transcriptional signatures at
3 (**F**) and 7 (**G**) days after SBI with and without injection. Supervised heatmap of fold
changes for SKM and saline with respect to untreated SBI at 3 (**H**) and 7 (**I**) days. $n = 6$
per group for histological assessments and 8 or 9 per group for gene expression analyses.

P values derived from one- or two-way ANOVA followed by pairwise comparisons with Tukey's or Šidák range test for parametric data, respectively, and Kruskal-Wallis followed by pairwise comparisons with Dunn's test for nonparametrically distributed data. Gene expression analysis was analyzed on the basis of NanoStringDiff package in R. *$P < 0.05$, **$P < 0.01$, and ****$P < 0.0001$; mean ± SEM, median (interquartile range).
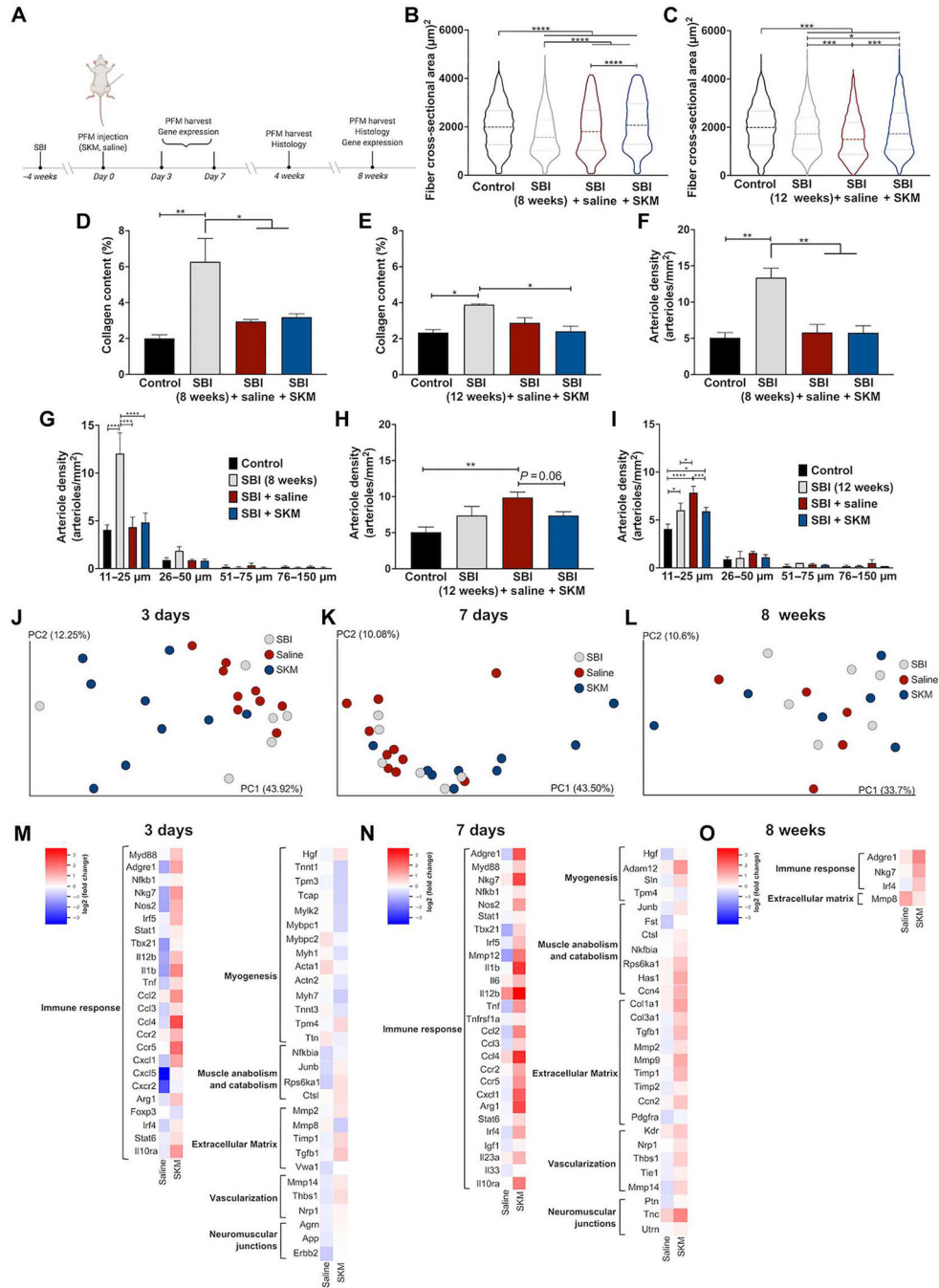
Fig. 7. Delayed injection of SKM prevents PFM atrophy and mitigates fibrosis.

(**A**) Study timeline. Pubocaudalis muscles of uninjured controls and animals subjected to SBI, SBI + saline injection, or SBI + SKM injection were compared with respect to fiber cross-sectional area at 4 weeks (**B**) or 8 weeks (**C**) after injection; collagen content (**D** and **E**); overall vessel density and vessel density separated by size at 4 weeks (**F** and **G**) and 8 weeks (**H** and **I**) after injection. PC analysis of transcriptional signatures at 3 (**J**) and 7 (**K**) days and 8 weeks (**L**) after injection (31 and 35 days and 12 weeks after SBI) with and without injection. Supervised heatmap of fold changes for SKM and saline with

respect to untreated SBI at 3 (**M**), 7 (**N**) days, and 8 weeks (**O**) after injection. $n = 6$ per group for histological assessments and 6 to 10 per group for gene expression analyses (both biological replicates). *P* values derived from one- or two-way ANOVA followed by pairwise comparisons with Tukey's or Šidák range test, respectively, for parametric data and Kruskal-Wallis followed by pairwise comparisons with Dunn's test for nonparametrically distributed data. Gene expression analysis was analyzed on the basis of NanoStringDiff package in R. *$P < 0.05$, **$P < 0.01$, ***$P < 0.001$, and ****$P < 0.0001$; mean ± SEM, median (interquartile range).